DOI 10.5012/bkcs.2010.31.5.1128

Relative Photonic Properties of Fe/TiO_2-Nanocarbon Catalysts for Degradation of MB Solution under Visible Light

Won-Chun Oh,[†,*] Feng-Jun Zhang,[†,‡] Ze-Da Meng,[†] and Kan Zhang[†]

[†]*Department of Advanced Materials & Science Engineering, Hanseo University, Chungnam 356-706, Korea*
[‡]*Anhui Key Laboratory of Advanced Building Materials, Anhui University of Architecture, Anhui Hefei 230022 P. R. China*
Received December 16, 2010, Accepted February 23, 2010

Nanocarbon supported Fe/TiO_2 composite catalysts were prepared using CNTs (carbon nanotubes) and C_{60} (fullerene) as nanocarbon sources by a modified sol-gel method. The Fe/TiO_2-nanocarbon composites were characterized by the BET surface area, scanning electron microscope (SEM), Transmission Electron Microscope (TEM), X-ray diffraction (XRD), energy dispersive X-ray (EDX) and UV-vis spectra. In comparison with non-nanocarbon doped Fe/TiO_2 composites, the nanocarbon supported Fe/TiO_2 composites had higher absorption ability with a larger specific surface area, and showed higher photocatalytic activity during the degradation of methylene blue (MB) under visible light. The reasons for the obvious increase of photocatalytic activity indicated that the photoactivity not only benefits from nanocarbon introduced, but also relates to the cooperative effect of the Fe as a dopant.

Key Words: Fe/TiO_2-nanocarbon composites, Photocatalytic activity, Visible light, MB

Introduction

Metal ions dopants with TiO_2 photocatalyst have been widely applied to extend the shift of photoreponse towards visible range of TiO_2. It was reported that Fe^{3+} dopant proved to be better than Cr^{3+}, Ni^{2+} and Zn^{2+} by contrastive effects among of different metals on the photoreactivity of TiO_2.[1] Otherwise, Fe^{3+} ion with the band gap of 2.6 eV seems to be an interesting dopant, which can extend the adsorption threshold towards visible range.[2,3] It had been proved that doping of low concentrations of Fe^{3+} cations can change the dynamics of the photocatalytic processes and substantially reduce the recombination process between dopant cation and titania matrixes.[4] Although Fe^{3+} modified TiO_2 photocatalysts are active under visible light irradiation, the efficiency is still low for practical use.[5] At the same time, the photocatalytic processes, mechanisms and kinetics on the doped TiO_2 are complex physical process and often make it difficult to draw the uniform conclusions, which lead to the controversies.

Recently, doping nonmetal atoms, such as C,[6] N[7] and S[8] have received much attention. Theoretical calculations showed that the p-orbitals of these dopants significantly overlapped with the valence band O 2p-orbitals, which facilitated the transport of photo-generated charge carriers to the surface of the catalyst. Especially, some authors reported the shift of photo response of TiO_2 from UV to the infrared region by a carbon dopant.[9] However, the enhancement of activity on TiO_2 is still slight.

Thus, it is of great interest to investigate the synergetic effect of multiple dopants. C and Fe co-doped TiO_2 showed higher activity than pristine TiO_2 in multiple uses.[10] Another previous research also showed two dopants had more beneficial effect than a single one for improving adsorption ability and photocatalytic activity under the visible light irradiation.[11] Generally, many parameters for photocatalytic activity such as the optical shift, photonic activity, surface area are important. Thus, in the field of carbon modified TiO_2, the use of nano-size carbon as CNTs and C_{60} have gained in popularity in recent years due to their unique properties.[12,13] The characteristic electronic properties of CNTs are that they can be either metallic or semiconducting, depending on their geometry.[14] C_{60} have energy-sensitizing capabilities for improving quantum efficiency and the increase in charge transfer between the fullerene and TiO_2.[15] In this work, the nanocarbon deposited with Fe/TiO_2 were synthesized by a two-step sol-gel process, and the application of these photocatalysts are here extended for the first time to visible light photodegradation of MB solution.

Experimental

Materials. CNT (Carbon nano-material Technology Co., Korea) and C_{60} (Tokyo Kasei Kogyo Co. Ltd., Japan) as the support material for preparation of Fe/TiO_2-nonocarbon were purchased, and used without further purification. *m*-chloroperbenzoic acid (MCPBA) was used as an oxidized reagent which was purchased from Acros Organics (New Jersey, USA). Benzene (99.5%) was used as an organic solvent which was purchased from Samchun Pure Chemical Co., Ltd. (Korea). TNB ($C_{16}H_{36}O_4Ti$) as a titanium dioxide source for the preparation of the Fe/TiO_2-nanocarbon composites was purchased from Aldrich Chemical Co., Ltd. (USA), and $Fe(NO_3)_3{\cdot}9H_2O$ as the ferric source was purchased from Duksan Pure Chemical Co., Ltd. (Korea). Analytical grade MB (99.99+%) was used and was purchased from Duksan Pure Chemical Co., Ltd. (Korea).

Preparation of samples. Fe/TiO_2 composites were performed by TNB as TiO_2 source with aqueous solutions of Fe $(NO_3)_3$ by a sol-gel method. The 3 mL TNB was dissolved in 20 mL of benzene to prepare the TNB solution. The 5 mL 0.1 M $Fe(NO_3)_3$ solutions were slowly dropped into the TNB solution prepared and vigorously stirred at 353 K for 5 h. The solution transformed to Fe/TiO_2 sol state, and was then dried at 363 K. Finally, the mixture was heat treated at 873 K. For preparation of Fe/TiO_2-nanocarbon composites, first, 2 g MCPBA was dissolved in

80 mL benzene. And then, 20 mg CNT or C_{60} powder was put into the oxidizing agent solution, refluxed at 353 K for 6 h then the solid precipitates were formed and dried at 363 K. The oxidized CNT or C_{60} was added into to the same amount of Fe $(NO_3)_3$ solutions as Fe/TiO_2 composites prepared, and the mixtures were stirred for 24 h using a non-magnetic stirrer at room temperature. After the heat treatment at 773 K, the Fe-nanocarbon was obtained. The Fe-nanocarbon was put into the TNB solution prepared as above and then the mixed solution was stirred for 5 h in an air atmosphere. After stirring the solution transformed to gel state, and these gels were reacted at 873 K for 1 h. The Fe/TiO_2-nanocarbon composites were then obtained. The procedure of prepared samples is showed in Fig 1.

Characteristics and investigations of the samples. The BET surface area by N_2 adsorption method was measured at 77 K using a BET analyzer (Monosorb, USA). XRD (Shimadz XD-D1, Japan) result was used to identify the crystallinity with Cu Kα radiation. SEM was used to observe the surface state and structure of Fe/TiO_2-nanocarbon composites using an electron microscope (JSM-5200 JOEL, Japan). TEM (JEOL, JEM-2010, Japan) at an acceleration voltage of 200 kV was used to investigate the size and distribution of the ferric and titanium deposits on the CNT or C_{60} surface of various samples. TEM specimens were prepared by placing a few drops of the sample solution on a carbon grid. EDX spectra were also obtained for determining the elemental information of Fe/TiO_2-nanocarbon composites. UV-vis absorption parameters for the MB solution decomposed by Fe/TiO_2 and Fe/TiO_2-nanocarbon composites were recorded by a UV-vis (Optizen Pop Mecasys Co., Ltd., Korean) spectrophotometer.

Photocatalytic activity of samples. The photocatalytic decomposition was tested by Fe/TiO_2 and Fe/TiO_2-nanocarbon composite powder and an aqueous solution of MB in a 100 mL glass container and then irradiation system with visible light (8W), which was used at a distance of 100 mm from the solution in dark box. The Fe/TiO_2 or Fe/TiO_2-nanocarbon composites (0.05 g) were suspended in 50 mL of MB solution with a concentration of 1.0×10^{-5} M. Then, the mixed solution was emplaced in the dark for at least 2 h, in order to establish an adsorption-desorption equilibrium, which was hereafter considered as the initial concentration (c_0) after dark adsorption. Experiments were then carried out under UV or under visible light. Solution was withdrawn regularly from the reactor by an order of 30 min, 60 min, 90 min, and 120 min. The 10 mL of solution was taken out and immediately centrifuged to separate any suspended solid. The clean transparent solution was analyzed by a UV-vis spectrophotometer. The blue color of the solution faded gradually with time due to the adsorption and decomposition of MB. Then, the concentration of MB in the solution was determined as a function of irradiation time from the absorbance change at a wavelength of 660 nm.

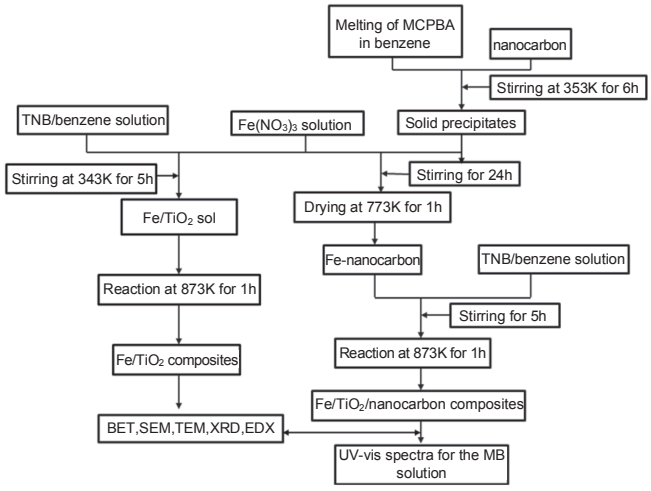

Figure 1. The preparation procedure of Fe/TiO_2 and Fe/TiO_2-nanocarbon composites.

Results and Discussion

BET surface area analysis. The values of the BET surface area of pristine TiO_2, Fe/TiO_2 and Fe/TiO_2-nanocarbon samples are presented in Table 1. As the results of Table 1, The BET surface areas of pristine TiO_2 and Fe-TiO_2 were 8.3 and 11.9 m^2/g, respectively. The BET surface areas of Fe/TiO_2-CNT and Fe/TiO_2-C_{60} increased to 58.7 and 31.2 m^2/g, respectively. When CNT and C_{60} compounds were introduced in Fe/TiO_2 composites, it can be evidently seen that there was large change of the micropore size distribution for Fe/TiO_2-CNT and Fe/TiO_2-C_{60} composites compared to that of corresponding Fe/TiO_2. This indicated that the supported CNT and C_{60} were directly related to adsorption ability of TiO_2.

SEM and TEM analysis. The SEM images of the Fe/TiO_2 and Fe/TiO_2-nanocarbon composites are shown in Fig. 2. SEM images of Fe/TiO_2 composites are shown in Fig 2 (a) and (b). The global and unequal size particles are coherent together. It is clear that the surface of the Fe/TiO_2 composites has densely packed flat pieces composed of the aggregation of nanoparticle TiO_2. The ultra structure was acquired on the outer Fe/TiO_2-C_{60} surface, as shown in Fig. 2 (c) and (d). The TiO_2 grain structure

Table 1. BET surface area and EDX elemental microanalysis (wt %) of pure TiO_2, Fe/TiO_2 and Fe/TiO_2-nanocarbon composites

Samples	S_{BET} (m^2/g)	Elements (wt %)			
		C	O	Ti	Fe
$Fe(NO_3)_3$ + TNB	11.9	0.00	55.5	43.4	1.11
C_{60} + $Fe(NO_3)_3$ + TNB	31.2	20.1	41.0	37.8	1.08
CNT + $Fe(NO_3)_3$ + TNB	58.7	22.5	36.8	39.6	1.10
Pure TiO_2	8.3	0.00	19.6	80.4	0.00

Table 2. Photodegradation rate constant of pure TiO_2, Fe/TiO_2 and Fe/TiO_2-nanocarbon composites

Samples	K_{app} (min^{-1})
Pure TiO_2	3.14×10^{-4}
Fe/TiO_2	2.46×10^{-3}
Fe/TiO_2-C_{60}	3.73×10^{-3}
Fe/TiO_2-CNT	4.38×10^{-3}

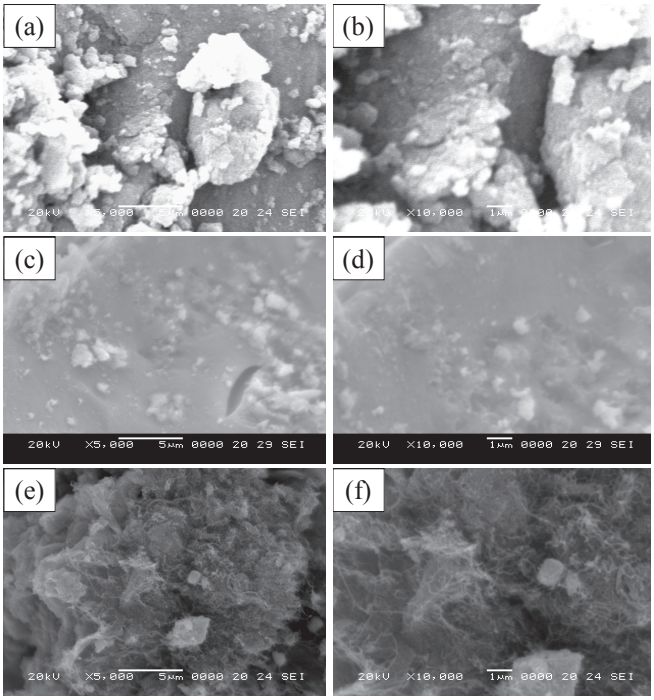

Figure 2. SEM micrographs of Fe/TiO_2 and Fe/TiO_2-nanocarbon composites: Fe/TiO_2: (a) ×5000, (b) ×10000, Fe/TiO_2-C_{60}: (c) ×5000, (d) ×10000 and Fe/TiO_2-CNT: (e) ×5000, (f) ×10000.

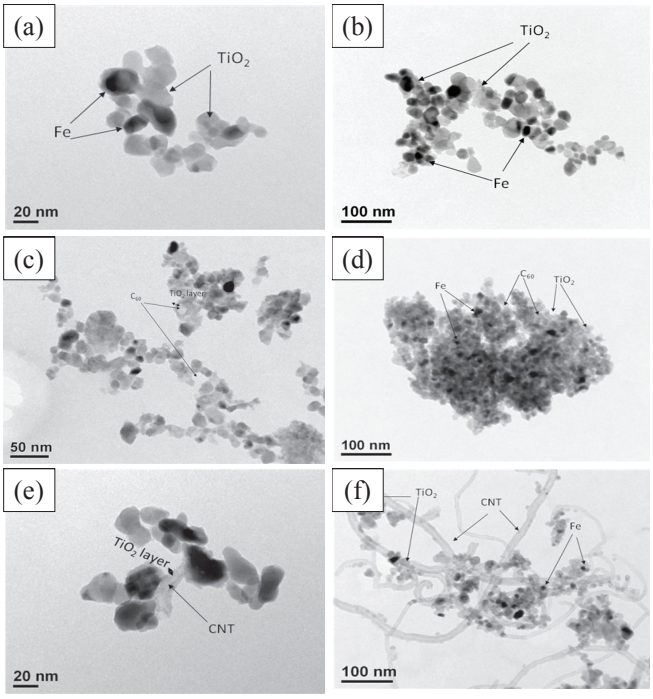

Figure 3. TEM micrograph of the Fe/TiO_2 and Fe/TiO_2-nanocarbon composites: (a) and (b): Fe/TiO_2, (c) and (d): Fe/TiO_2-C_{60}, (e) and (f): Fe/TiO_2-CNT.

is clearly visible with a great distribution on C_{60} surface due to considerable portion of TiO_2 attached in the 3-D matrix. However, these TiO_2 particles have a large size in clusters and agglomerate shape. But the rough grain structure can be considered to provide an ideal entrance pathway for diffusion of oxygen and organic molecules between the grains and C_{60}. The morphological characterization of the Fe/TiO_2-CNT composites was present in Fig 2 (e) and (f). These micrographs showed the general morphology of CNT, and which was decorated with will-dispersed TiO_2 particles. However, small amounts of TiO_2 particles were also aggregated to be bundles, which possibly are not well homogenized during vigorous stirring. It was considered that better dispersion enables larger number of active catalytic centers for the photocatalytic reaction.[16]

It was not exactly clear which nanocarbon was present within SEM images, so the TEM images were further complicated by the fact that the higher nanocarbons exhibited multiple isomeric forms with shapes ranging from approximately ellipsoidal to spheroidal for C_{60} and a wall tube for CNT as shown in Figs. 3 (c)-(f). The TEM images of Fe/TiO_2 are shown in Fig. 3 (a) and (b), which showed that the size of TiO_2 particle observed was about 10 ~ 20 nm. Moreover, a few black dots were observed from the image, they correspond to the deposition of Fe particles. The Fe/TiO_2-nanocarbon composites were investigated by TEM to obtain additional information about the interfacial region of the C_{60} and CNT crystals and surface areas. It revealed a generally precipitate-free and smooth interface between the Fe and TiO_2 matrix and the C_{60} crystals, as shown in Figs. 3 (c) and (d). Occasionally a 0.1 - 0.5 nm thin layer was observed at the periphery of the C_{60} crystals. The Figs. 3 (e) and (f) show that the surface areas of Fe/TiO_2-CNT composites should be a strong interphase structural effect between the carbon and metal oxide phases. A homogeneous dispersion of CNT in TiO_2 matrix implied a possible disappearance of CNT characteristic peaks in their XRD patterns. According to the previous study,[17] the homogeneous distribution of TiO_2 on the nanocarbon external surface could be formed by the MCPBA oxidation method. The black dots distributed in Fig. 3 (c)-(f) also corresponded to the Fe particles. It was considered that there is evidence of the formation of Fe doped TiO_2 outside the pores in some segments. This was possibly associated with the formed crystalline of Fe and TiO_2, which was also agreed with their XRD results.

XRD analysis. The XRD patterns are given in Fig. 4. The Fe-nanocarbon presented that the intense peaks of CNT and C_{60} correspond to the (002) reflection and to the (10) band. In the case of the Fe/TiO_2-nanocarbon composites, the additional peaks presented in all the diffractograms correspond to the single anatase form of TiO_2. It was noticed that the (101) anatase reflection overlaps the (002) reflection of nanocarbon. The XRD results illuminated that the nanocarbon in Fe/TiO_2-nanocarbon composites is coated with a typical single anatase crystallites. In XRD patterns of the Fe/TiO_2, significant diffraction peaks of rutile-phase TiO_2 were detected. It reflected that the nanocarbon suppressed phase transformation from anatase to rutile during heat treatment at high temperature. According to the former study,[18] pure anatase nanocrystallites are very efficient photocatalysts and have superior photocatalytic properties. Especially, pure maghemite (γ-Fe_2O_3) (JCPDS card no. 19-0629) could be obtained from only Fe-nanocarbon composites.[19] In comparison of Fe/TiO_2 and Fe/TiO_2-nanocarbon composites, there was significantly difference. It is noteworthy that uniform peaks of '$FeO+2TiO_3$' were detected in both Fe/TiO_2 and Fe/

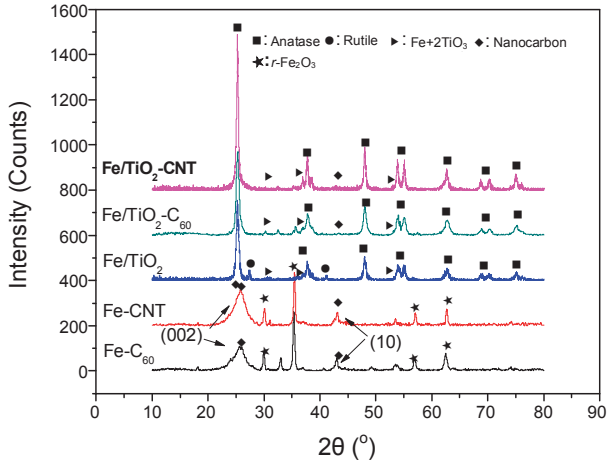

Figure 4. XRD patterns of Fe-nanocarbon, Fe/TiO_2 and Fe/TiO_2-nanocarbon composites.

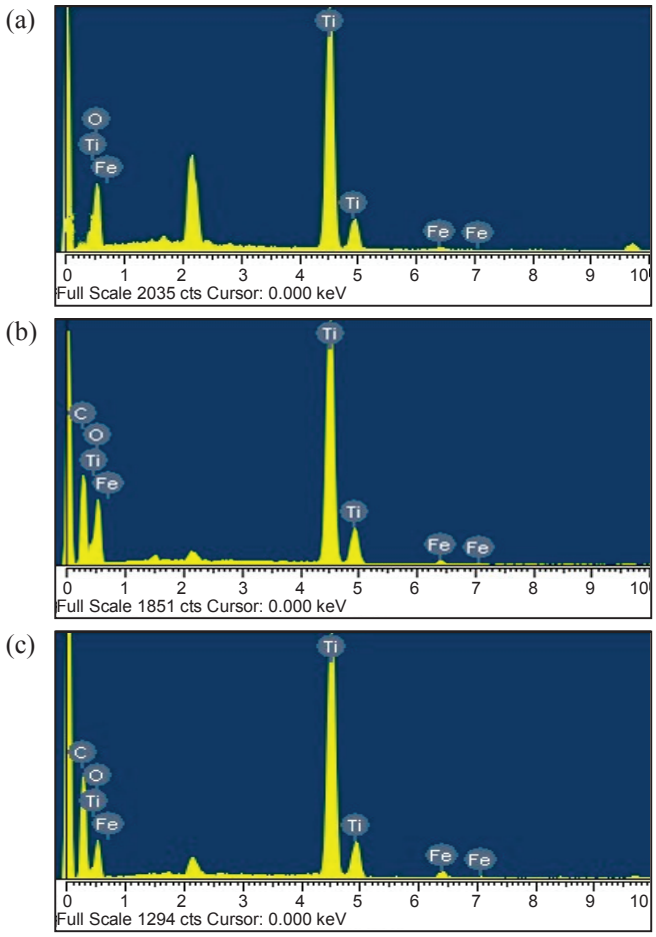

Figure 5. EDX elemental microanalysis of Fe/TiO_2 and Fe/TiO_2-nanocarbon composites: (a) Fe/TiO_2, (b) Fe/TiO_2-C_{60}, and (c) Fe/TiO_2-CNT.

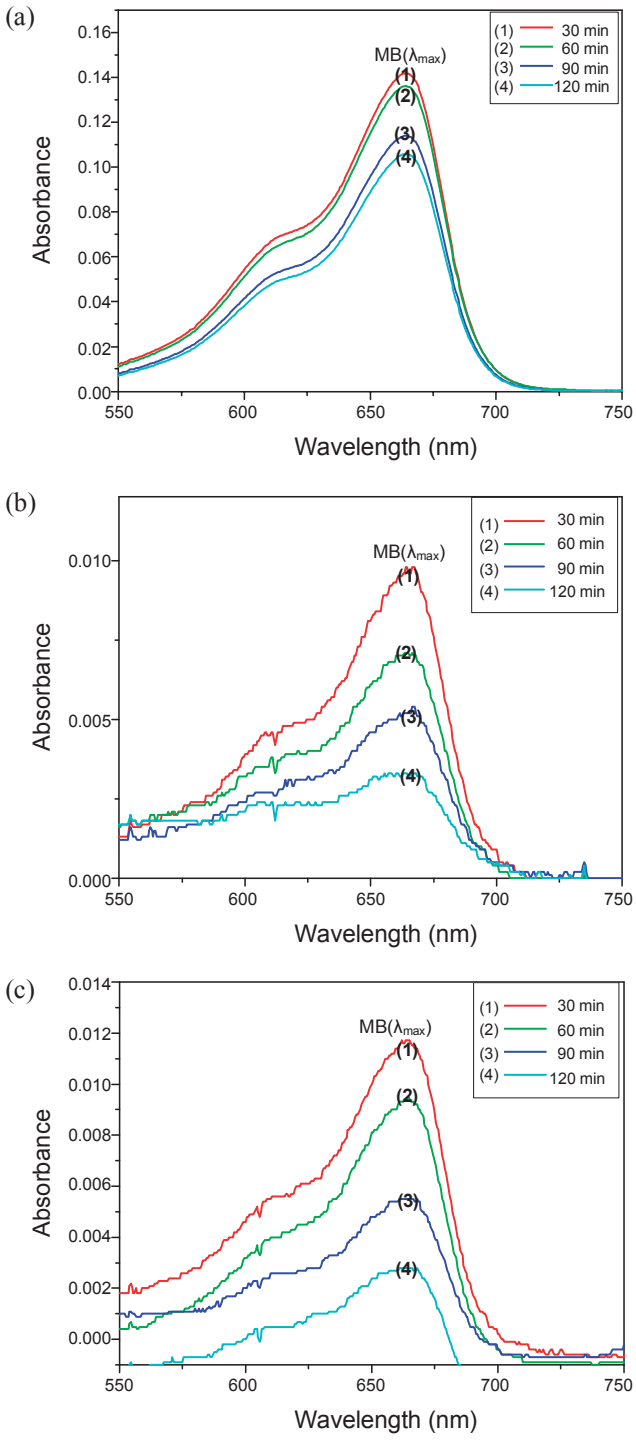

Figure 6. Absorption spectral changes of MB in the Fe/TiO_2 and Fe-nanocarbon composites as a function of irradiation time (visible light). (a): Fe/TiO_2, (b): Fe/TiO_2-C_{60} and (c): Fe/TiO_2-CNT.

TiO_2-nanocarbon composites, which indicated that the Fe/TiO_2 was successfully deposited on nanocarbon surface by our experimental method. It was considered that the addition of TNB results in phase transformation from γ-Fe_2O_3 to FeO+2TiO_3 during reaction at high temperature.

EDX analysis. Fig 5 shows the results of the EDX for Fe/TiO_2-nanocarbon and Fe/TiO_2 composites. These spectra showed the presence of peaks from the C, O, Ti and Fe elements, and the numerical contents for the various elements are listed in Table 3. The quantities of carbon and Fe in the Fe/TiO_2-nanocarbon composites were small with a major element of Ti. According to former studies,[4,20] the higher concentration of

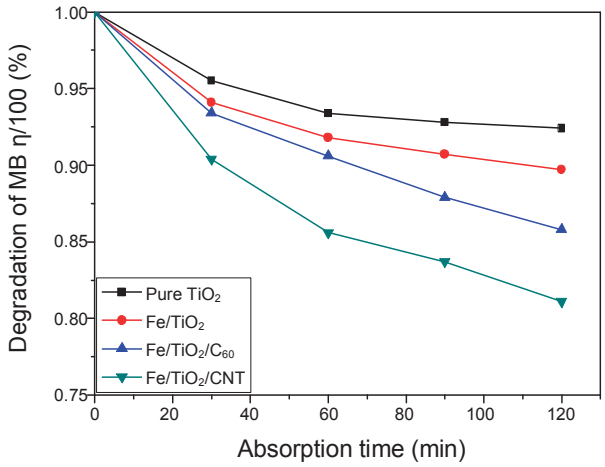

Figure 7. Adsorption capability of pure TiO_2, Fe/TiO_2, and Fe/TiO_2-nanocarbon for MB dyes under dark condition. η

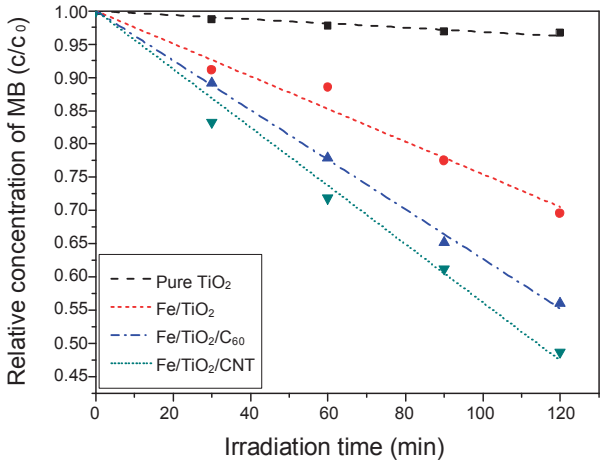

Figure 8. Apparent first order kinetics of MB degradation for pure TiO_2, Fe/TiO_2, and Fe/TiO_2-nanocarbon composites.

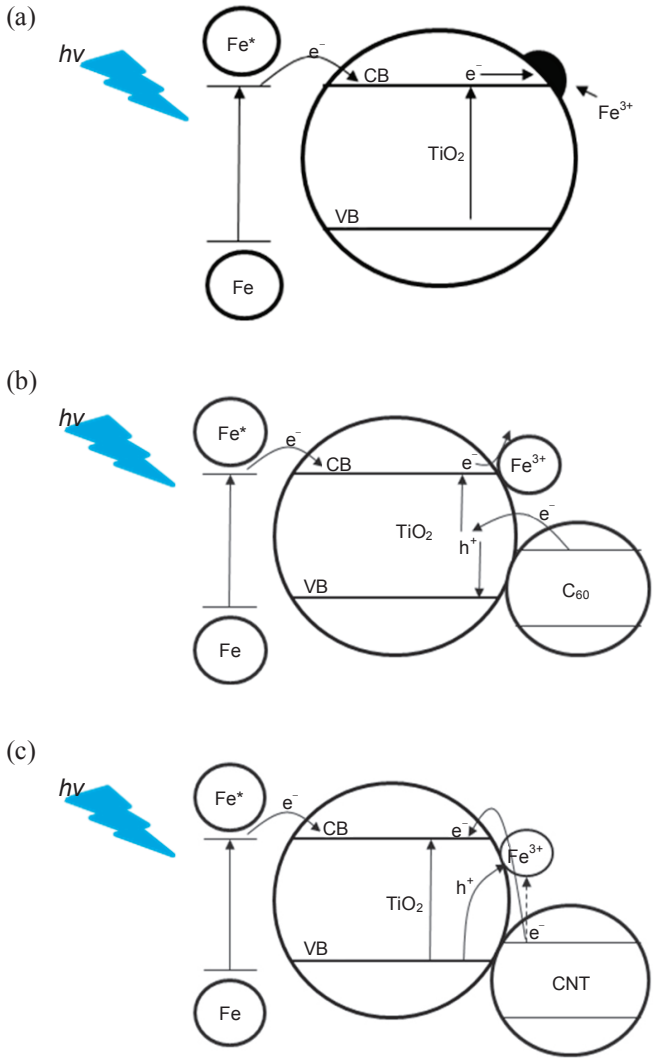

Figure 9. Schematic diagram of Fe/TiO_2, Fe/TiO_2-nanocarbon and initial electrons excited process after activation by visible light. (a): Fe/TiO_2, (b): Fe/TiO_2-C_{60} and (c): Fe/TiO_2-CNT.

dopant in TiO_2 matrix can be detrimental in formation of hole/electron recombination centers and an increase of negative charge capabilities.

Photocatalytic activity of the Fe/TiO_2 and Fe/TiO_2-nanocarbon composites. The photocatalytic activity of the Fe/TiO_2 and Fe/TiO_2-nanocarbon composites was assessed from the kinetics of the photodegradation of MB solution under visible light. An initial concentration of 1×10^{-5} mol/L for MB solution and a maximum reaction time of 2 h were experimentally determined. The spectral changes of MB in the Fe/TiO_2 and Fe/TiO_2-nanocarbon composites are shown in Fig. 6. The UV-vis absorption spectra in Fig. 6 gave absorption maximum values at a wavelength of 660 nm simultaneously with a large decrease in the absorbance as a function of irradiation time.

The adsorption abilities of pure TiO_2, Fe/TiO_2 and Fe/TiO_2-nanocarbon composites were evaluated within 120 min before the visible light excitation. It was quite easy to draw a causal relationship between surface areas in Table 1 and adsorption efficiency in Fig. 7. From the Fig 7, it was clear that degradation of MB on Fe/TiO_2 composites is faster than that of pure TiO_2 powder. This can be attributed to the high porosity of Fe/TiO_2 surface due to introduction of Fe component, which correlated with an increase of adsorption ability. For higher absorption capability of Fe/TiO_2-nanocarbon composites, a direct cause in nanocarbon themselves had a high pore value.

The photocatalytic activities of the pure TiO_2, Fe/TiO_2 and Fe/TiO_2-nanocarbon composites were tested on the photocatalytic degradation of MB solution under visible light irradiation as a test reaction. Fig. 8 shows that the Fe/TiO_2 exhibited a much higher activity than undoped TiO_2, and the Fe/TiO_2-nanocarbon composites exhibited a higher activity than Fe/TiO_2 composites. To quantitatively evaluate the photocatalytic activities of samples, the kinetics of photodegradation of MB over the above samples were studied. The photocatalytic degradation reaction with suspended samples approximately obeys the first-order kinetics. The representation for the rates of degradation of MB is given by:

$$\ln (C/C_0) = kt_0$$

Where C and C_0 are the initial concentration of MB, t_0 is the irradiation time, and k denotes the overall degradation rate constant. By plotting ln (C/C_o) as a function of time through regression, the k (min^{-1}) constant for each samples was obtained from the slopes of the simulated straight lines, as listed in Table 2. According to results in Table 2, the Fe/TiO_2 composites showed a higher enhancement in the MB photodegradation than that of pure TiO_2, which illuminated that Fe dopant is one of the vital factors in determining the photocatalytic activity of the catalysts under visible light. We also can see that the nanocarbon can be definite benefiter for photocatalytic activity. The photocatalytic activities of Fe/TiO_2-nanocarbon composites were significant higher than that of Fe/TiO_2 composites.

Effects of Fe and nanocarbon under visible light irradiation. The photocatalytic activities of Fe/TiO_2 for the degradation of MB were enhanced by the Fe dopant through the following mechanisms as shown in Fig 9 (a). First, Fe particles dopant on TiO_2 acted as electron traps, enhancing the electron-hole separation and the subsequent transfer of the trapped electron to the adsorbed O_2 acting as an electron acceptor.[21,22] Second, the surface plasmon resonance of Fe particles is excited by visible light, facilitating the excitation of the surface electron and interfacial electron transfer. [23]

The significantly enhanced photodegradation of MB in the Fe/TiO_2-nanocarbon composites under visible light irradiation may be ascribed to the cooperative effect of Fe and nanocarbon dopants, as shown in Figs. 9 (b) and (c). The photodegradation rate kinetic of the C_{60} and CNT was different due to their different nanostructures.

Kamat *et al*. reported that C_{60} could accept electron or donate electron to the TiO_2 semiconductor depending on different conditions.[24,25] Basically, TiO_2 leads to the trapping of holes and electrons which can be suppressed by C_{60} under UV irradiation.[24] Simultaneously, C_{60} could also donate electron to TiO_2 semiconductor. Moreover, in the previous study,[26] the Pt treated C_{60}/TiO_2 composites could powerfully degrade the organic dye by the organo-metallic reaction on the Pt compound and energy transfer effects such as quantum efficiency of the fullerene. It suggested that the metal in C_{60}/TiO_2 matrix can act as electron recipient to cooperate with C_{60} under UV irradiation. In this case, excitation of visible light injects electrons from Fe-C_{60} to TiO_2 through a biphotonic electron ejection mechanism. This can be seen in Fig. 9 (b), when the light impinges on Fe/TiO_2-C_{60} composites, C_{60} and Fe can be excited to simultaneously generate electron in the visible region. Especially, the excited C_{60} can inject one electron to the separated hole of TiO_2. This can be represented by the following reaction:

$$TiO_2 (hole) + C_{60}^* \rightarrow TiO_2 + C_{60}^+$$

Where the hole generated can combine with electrons injected by C_{60} into the valence band, hence the electron generated is promoted to conduction band, which results in photocurrent increase. In addition, the Fe particles on the TiO_2 surface can also act as electron traps facilitating the electron transfer.

An *et al*. reported that CNT may absorb the irradiation and transfer the photo-induced electron (e^-) into the conduction band of the TiO_2 particles.[27,28] Their study showed that the photo generation of charges involving CNT was the major contribution to the photo action spectrum. As for present experiment, Fe-CNT is energetic enough and read to inject one electron through the coordinating bands to the conduction band of TiO_2 as shown in Fig 9 (c). In addition, with substitution for oxygen atoms by the CNT and Fe in the anatase crystal structure of TiO_2, new levels are introduced between the conduction and valence band of TiO_2, the electrons generated by TiO_2 can be promoted from the valence band to CNT level introduced by Fe dopant, or from the lower to the higher CNT levels, which results in the quantities of electrons increase. Therefore, the Fe/TiO_2-CNT composites had a narrower band gap than Fe/TiO_2 and could increase the absorption in the visible-light region. The departed holes may migrate to the surface of Fe particles.

Conclusion

In this research, composites of Fe/TiO_2 supported on a nanocarbon surface were successfully prepared by a modified sol-gel method. Only the anatase phase was detected by XRD results for Fe/TiO_2-nanocarbon composites. Otherwise, it was clearly seen that the Fe/TiO_2 and Fe/TiO_2-nanocarbon composites had the same crystalline $Fe+2TiO_3$. According to the results of the photodegragation of MB, the Fe/TiO_2-nanocarbon composites showed that they could absorb more photoenergy in the visible light region and had a greater surface area than Fe/TiO_2. The high activity was attributed to several different beneficial effects associated with the introduction of C_{60} and CNT.

Reference

1. Ghasemi, S.; Rahimnejad, S.; Setayesh, S. R.; Rohani, S.; Gholami, M. R. *J. Hazar. Mater.* **2009**, *172*, 1573.
2. Navio, J. A.; Macia,s M.; Gonzalez-Catalan, M.; Justo, A. *J. Mater. Sci.* **1992**, *27*, 3036.
3. Bickley, R. I.; Lees, J. S.; Tilley, R. J. D.; Palmisano, L.; Schiavello, M. *J. Chem. Soc. Faraday. Trans.* **1992**, *88*, 377.
4. Hung, W. C.; Chen, Y. C.; Chu, H.; Tseng, T. K. *Appl. Sur. Sci.* **2008**, *255*, 2205.
5. Yang X. X.; Cao, C. D.; Erickson, L.; Hohn, K.; Maghirang, R.; Klabunde, K. *Appl. Catal. B. Env.* **2009**, *91*, 657.
6. Tachikawa, T.; Tojo, S.; Kawai, K.; Endo, M.; Fujitsuka, M.; Ohno, T.; Nishijima, K.; Miyamoto, Z.; Majima, T. *J. Phys. Chem. B* **2004**, *108*, 19299.
7. Asahi, R.; Morikawa, T.; Ohwaki, T.; Aoki, A.; Taga, Y. *Sci.* **2001**, *193*, 269.
8. Ohno, T.; Mitsui, T.; Matsumura, M. *Chem. Lett*. **2003**, *32*, 364.
9. Wang, X.; Meng, S.; Zhang, X.; Wang, H.; Zhang, W.; Du, Q. *Chem. Phys. Lett.* **2007**, *444*, 292.
10. Tryba, B. *J. Hazard. Mater.* **2008**, *151*, 623.
11. Yang, X.; Cao, C.; Hohn, K.; Erickson, L.; Maghirang, R.; Klabunde, K. *J. Catal.* **2007**, *252*, 296.
12. Oh, W. C.; Jung, A. R.; Ko, W. B. *Mater. Sci. Eng. C* **2009**, *29*, 1338.
13. Zhang, F. J.; Chen, M. L.; Oh, W. C. *Bull. Korean Chem. Soc.* **2009**, *30*, 1798
14. Cao, G. *Nanostructures & Nanomaterials*; Imperial College Press: London 2004, 344.
15. Oh, W. C.; Jung, A. R.; Ko, W. B. *J. Ind. Eng. Chem.* **2007**, *13*, 1208.
16. Zhang, Y.; Kohler, N.; Zhang, M. Q. *Biomater.* **2002**, *23*, 1553.
17. Oh, W. C.; Chen, M. L. *Bull. Korean Chem. Soc.* **2008**, *29*, 159.

18. Chen, M. L.; Bae, J. S.; Oh, W. C. *Anal Sci& Technol*. **2006**, *19*, 460.
19. Neri, G.; Visco, A. M.; Galvagno, S.; Donato, A.; Panzalorto, M. *Thermochimica Acta* **1999**, *329*, 39.
20. Chen, L.C.; Ho, Y.C.; Guo, W.S.; Huang, C. M.; Pan, T. C. *Electrochimica Acta* **2009**, *54*, 3884.
21. Pera-Titus, M.; García-Molina, V.; Baños, M. A.; Giménez, J.; Esplugas, S. *Appl. Catal. B. Env.* **2004**, *47*, 219.
22. Neamtu, M.; Yediler, A.; Siminiceanu, I.; Kettrup, A. *J. Photochem. Photobiol. A* **2003**, *161*, 87.
23. Tu, Y. F.; Huang, S. Y.; Sang, J. P.; Zou, X. W. *Mater. Res. Bull.* **2009**, doi:10.1016/j.materresbull.2009.08.020.
24. Kamat, P.V.; Gevaert, M. *J. Phys. Chem. B* **1997**, *101*, 4422.
25. Kamat, P. V.; Bedja, I.; Hotchandani, S. *J. Phys. Chem.* **1994**, *98*, 9137.
26. Oh, W. C.; Ko, W. B. *J. Ind. Eng. Chem.* **2009**, *15*, 791.
27. An, G. M.; Ma, W. H.; Sun, Z. Y.; Liu, Z. M.; Han, B. X.; Miao, S. D.; Miao, Z. J.; Ding, K. L. *Carbon* **2007**, *45*, 1795.
28. Chen, M. L.; Zhang, F. J.; Oh, W. C. *New Carbon Materials* **2009**, *24*, 159.